JVI Journals.ASM.org

# Structures of the Compact Helical Core Domains of Feline Calicivirus and Murine Norovirus VPg Proteins

**Eoin N. Leen,[a] K. Y. Rex Kwok,[b] James R. Birtley,[a]* Peter J. Simpson,[b] Chennareddy V. Subba-Reddy,[f] Yasmin Chaudhry,[c]* Stanislav V. Sosnovtsev,[e] Kim Y. Green,[e] Sean N. Prater,[a]* Michael Tong,[a]* Joanna C. Young,[a] Liliane M. W. Chung,[c] Jan Marchant,[b] Lisa O. Roberts,[d] C. Cheng Kao,[f] Stephen Matthews,[b] Ian G. Goodfellow,[c]* Stephen Curry[a]**

Division of Cell and Molecular Biology, Department of Life Sciences, Imperial College London, London, United Kingdom[a]; Division of Biomolecular Science, Department of Life Sciences, Imperial College London, London, United Kingdom[b]; Section of Virology, Faculty of Medicine, Imperial College London, London, United Kingdom[c]; School of Biomedical and Molecular Sciences, University of Surrey, Guildford, Surrey, United Kingdom[d]; Laboratory of Infectious Diseases, National Institute of Allergy and Infectious Diseases, National Institutes of Health, Bethesda, Maryland, USA[e]; Department of Molecular and Cellular Biochemistry, Indiana University, Bloomington, Indiana, USA[f]

**We report the solution structures of the VPg proteins from feline calicivirus (FCV) and murine norovirus (MNV), which have been determined by nuclear magnetic resonance spectroscopy. In both cases, the core of the protein adopts a compact helical structure flanked by flexible N and C termini. Remarkably, while the core of FCV VPg contains a well-defined three-helix bundle, the MNV VPg core has just the first two of these secondary structure elements. In both cases, the VPg cores are stabilized by networks of hydrophobic and salt bridge interactions. The Tyr residue in VPg that is nucleotidylated by the viral NS7 polymerase (Y24 in FCV, Y26 in MNV) occurs in a conserved position within the first helix of the core. Intriguingly, given its structure, VPg would appear to be unable to bind to the viral polymerase so as to place this Tyr in the active site without a major conformation change to VPg or the polymerase. However, mutations that destabilized the VPg core either had no effect on or reduced both the ability of the protein to be nucleotidylated and virus infectivity and did not reveal a clear structure-activity relationship. The precise role of the calicivirus VPg core in virus replication remains to be determined, but knowledge of its structure will facilitate future investigations.**

Caliciviruses are a family of positive-sense, single-stranded RNA viruses that contain the *Vesivirus*, *Sapovirus*, *Lagovirus*, and *Norovirus* genera. They infect a wide variety of mammals, causing an array of different diseases. For example, feline calicivirus (FCV), a vesivirus, is associated with a range of conditions, including upper respiratory tract disease in cats (1), while noroviruses and sapoviruses cause gastroenteritis. Human noroviruses represent a major health problem: they are estimated to be responsible for 21 million cases of gastroenteritis in the United States every year and 200,000 deaths among children in developing countries (2, 3).

The study of human noroviruses (HuNV) has been impeded by the absence of a viable cell culture system for this pathogen and the fact that baby gnotobiotic pigs are the only available small-animal model (4, 5). As a result, other caliciviruses have often been used as surrogate models for the investigation of HuNV biology (6). FCV and murine norovirus (MNV) have been widely used to investigate general features of calicivirus replication since they both grow in tissue culture and have workable reverse genetics systems (7–11). MNV is emerging as a popular model system since it can cause systemic disease or gastroenteritis in immunocompromised mice that resembles human norovirus infections (12, 13).

The ~7.5-kb calicivirus genome contains 2 to 4 open reading frames (ORFs) depending on the genus. The major (VP1; ORF2) and minor (VP2; ORF3) capsid proteins of caliciviruses are usually translated from a subgenomic RNA (as is the protein derived from ORF4 in MNV [14]). ORF1 encodes a large polyprotein precursor that is cleaved into mature nonstructural proteins (NS1 to NS7) by the virus-encoded protease NS6$^{pro}$ (15–18). The mature proteins include an RNA-dependent RNA polymerase (RdRp) (NS7$^{pol}$), an ATPase (NS3), and proteins that disrupt cellular trafficking (NS1-2 and NS4) (18–23).

In addition, proteolytic cleavage of the ORF1 polyprotein releases the NS5 protein, which is also known as VPg (viral protein genome linked). The caliciviral VPg is a 13- to 15-kDa protein that is found covalently attached to the 5′ terminus of the genomic and subgenomic RNAs (24–26). Covalently attached terminal proteins are also found at the 5′ ends of the genomes of other positive-sense RNA viruses, including the *Picornaviridae* and *Astroviridae*, which are mammalian viruses, and several plant virus families, such as the *Potyviridae*, *Comoviridae*, and *Nepoviridae*. They also occur in DNA viruses in the *Adenoviridae* and in members of the bacteriophage *Podoviridae* (27–34).

The VPg proteins of different viruses vary in size and sequence. For example, within the positive-sense RNA viruses, *Comoviridae* and *Picornaviridae* VPgs are ~3 kDa, the *Potyviridae* VPg is ~24

**Received** 9 November 2012 **Accepted** 6 March 2013

**Published ahead of print** 13 March 2013

Address correspondence to Stephen Curry, s.curry@imperial.ac.uk.

* Present address: James R. Birtley, Pathology Department, University of Massachusetts Medical School, Worcester, Massachusetts, USA; Sean N. Prater, Division of Medical Genetics, Department of Pediatrics, Duke University Medical Center, Durham, North Carolina, USA; Michael Tong, Department of Pharmacology, Stony Brook University Medical School, Stony Brook, New York, USA; Yasmin Chaudhry and Ian G. Goodfellow, Division of Virology, Department of Pathology, University of Cambridge, Addenbrooke's Hospital, Hills Road, Cambridge, United Kingdom.



doi:10.1128/JVI.03151-12

The authors have paid a fee to allow immediate free access to this article.

kDa, and the *Calicivirus* VPg is 13 to 15 kDa. The calicivirus VPg proteins are more similar to the VPgs found in *Astroviridae*, which are predicted to be around 11 kDa in size and have 20 to 27% amino acid sequence identity with their calicivirus counterparts (28).

VPg is essential for translation initiation from genomic and subgenomic RNAs and appears to act as a cap substitute for ribosomal recruitment (8, 25). The molecular basis for this function is now emerging. The VPg proteins from both FCV and MNV have been found to interact with the cap-binding protein eIF4E (35, 36). In addition, an interaction has been demonstrated between HuNV VPg and purified eIF3 complex (37). These studies suggest that VPg may recruit the ribosome to the genomic RNA through interaction with the canonical translation initiation factors. A similar role has also been described for the VPg proteins from the *Nepoviridae* and *Potyviridae* (38–41). Moreover, the observations that protease K treatment to remove VPg from astrovirus RNA renders the viral RNA noninfectious and that infectivity can be restored to RNA transcripts by addition of a 5′ $m^7G$ cap are consistent with a role for astroviral VPg in translation (28, 42).

VPg is also important for genome replication. The caliciviral VPg can be nucleotidylated by the viral polymerase via a phosphodiester linkage to a conserved tyrosine residue (43)—Y24, Y26, and Y27 in the VPg of FCV, MNV, and human norovirus (HuNV), respectively (43–45). Nucleotidylated VPg can be extended in a template-dependent manner to produce RNA-linked VPg (46). While the mechanism of caliciviral RNA replication has not been fully characterized, it is likely that VPg becomes covalently attached to the genomic RNA by acting as a primer for positive-strand RNA synthesis. Yeast two-hybrid data also suggest that the FCV VPg protein interacts with the major capsid protein VP1, indicative of a possible role in the selective encapsidation of VPg-linked viral RNA (47).

The solution structures of the 22-amino-acid VPg from poliovirus, a picornavirus, have been determined using nuclear magnetic resonance (NMR) spectroscopy for both the native peptide and VPg that has been nucleotidylated on its acceptor Tyr 3 residue (48, 49). In its native form, poliovirus VPg appears to be highly flexible; a defined conformation was observed only in the presence of high concentrations (1 M) of the organic solvent trimethylamine *N*-oxide (TMAO). Intriguingly, the nucleotide-linked poliovirus VPg-pU appeared more stable and exhibited a defined, globular conformation in an aqueous solution that lacked TMAO (48). However, the physiological relevance of this structure is uncertain; although the poliovirus VPg-pU structure may be computationally docked with the viral three-dimensional (3D) polymerase, the resulting model did not position the uridine in VPg close enough to the active-site residues of the polymerase to plausibly account for the nucleotidylation reaction. Moreover, this model does not take into account the conformational changes that might be induced by association with the polymerase and is inconsistent with the extended conformation of VPg-pU observed in the crystal structure of the $3D^{pol}$-VPg-pU complex for the closely related picornavirus foot-and-mouth disease virus (FMDV) (50).

Both the potyviral and noroviral VPgs have been predicted to be largely disordered (51). In the case of potyviruses, circular dichroism and thermal stability measurements and tryptic digest assays all pointed to the presence of some structured elements within the protein (52–54). But although NMR analyses have detected several aromatic shifted methyl peaks in 1D and $^1H$-$^{13}C$ heteronuclear single quantum coherence (HSQC) spectra for potyvirus VPg, suggesting that the protein is at least partially folded (54), it is commonly regarded as "intrinsically disordered" (55).

We report here the determination of the solution structures of two calicivirus VPgs using NMR spectroscopy. We find that the FCV and MNV VPg proteins both possess a compact helical core that is flanked by unstructured N- and C-terminal tails. Intriguingly, the MNV VPg core contains only the first two of the three helices present in the core of FCV VPg. For both proteins, the nucleotidylated Tyr residue projects into solvent from the center of the first helix in the protein core. The core structure facilitated the design of mutagenesis experiments to investigate the role of the protein structure in RNA replication and infectivity. The results showed that mutations that disrupt the fold of the helical core generally impair the ability of VPg to support virus replication and nucleotidylation by the MNV VPg. The structured core therefore appears to be functionally important for interaction with the MNV RdRp.

## MATERIALS AND METHODS

**VPg cloning and expression.** MNV VPg 11-62, 11-85, and 1-124 (full length) were amplified from the MNV-1 infectious clone pT7:MNV 3′Rz (NCBI accession number DQ285629.1) and ligated into the expression vector pETM11 (7, 56). FCV VPg 1-111 (full length) was amplified from a full-length FCV VPg clone of the F9 strain (NCBI accession number M86379) and ligated into pETM11. FCV VPg 9-79 was amplified from the same template and ligated into the expression vector pQE30 (Qiagen). Both pQE30 and pETM11 encode N-terminal 6-histidine tags. Processing of proteins expressed from the pETM11 vector with tobacco etch virus (TEV) NIa protease removed the tag, leaving GAM and G residues on the N termini of MNV and FCV VPg, respectively. The pQE30 vector adds a noncleavable polyhistidine tag (MRGSHHHHHHGS) to the N terminus of the expressed protein.

QuikChange mutagenesis (Stratagene) was performed on pETM11 FCV VPg 1-111 and MNV VPg 1-124 constructs to produce the following mutants for NMR analyses: FCV VPg Y24A, F43A, R47E, F62A, and R69E and MNV VPg Y26A, Y26F, F29A, R32D, Y40A, Y40F, Y45A, Y45F, D48R, and the R32D D48R double mutant. The sequences of primers used for mutagenesis can be found at http://dx.doi.org/10.6084/m9.figshare.155873.

All isotopically labeled MNV VPg proteins were expressed in *Escherichia coli* (DE3) Rosetta cells for 16 to 18 h at 20°C by addition of isopropyl-β-D-thiogalactopyranoside (IPTG) to a final concentration of 1 mM. The MNV VPg 11-85 construct used for structure determination was expressed using *E. coli* OD 2 $^{13}C$, $^{15}N$-rich medium (Silantes), whereas $^{15}N$-labeled MNV VPg 1-124 and 11-62 were expressed in minimal medium containing 0.2% (wt/vol) $^{15}NH_4Cl$.

FCV VPg 1-111 protein for backbone assignment and $^1H$-$^{15}N$ heteronuclear nuclear Overhauser effect (hetNOE) analysis was expressed in *E. coli* BL21(DE3) cells for 4 h in *E. coli* OD 1 $^{13}C^{15}N$-rich medium (Silantes) at 22°C with 1 mM final IPTG. The FCV VPg 11-79 protein for the structure determination was expressed overnight in *E. coli* M15 in minimal medium containing 0.1% (wt/vol) $^{15}NH_4Cl$ and 0.4% (wt/vol) $^{13}C_6$ glucose at 18°C with 0.5 mM final IPTG. Unlabeled MNV VPg 1-124 and FCV VPg 1-111 and mutant variants of these proteins used in 1D NMR experiments were produced in *E. coli* (DE3) Rosetta cells for 4 h in lysogeny broth (LB) (57) at 20°C by addition of 1 mM IPTG.

**Protein purification.** Isotopically labeled MNV VPg proteins were purified by affinity chromatography using Talon resin (Clontech). The polyhistidine tag was then removed by overnight incubation with approximately 1 mg of polyhistidine-tagged TEV NIa protease per 15 mg of VPg in a buffer typically made up of 50 mM sodium phosphate (pH 6.5), 300 mM NaCl, and 1 mM dithiothreitol (DTT). TEV NIa protease and cleaved tags were removed from VPg by reapplication of the cleaved VPg to Talon. Final purification of MNV VPg 11-85 for the structure determination and

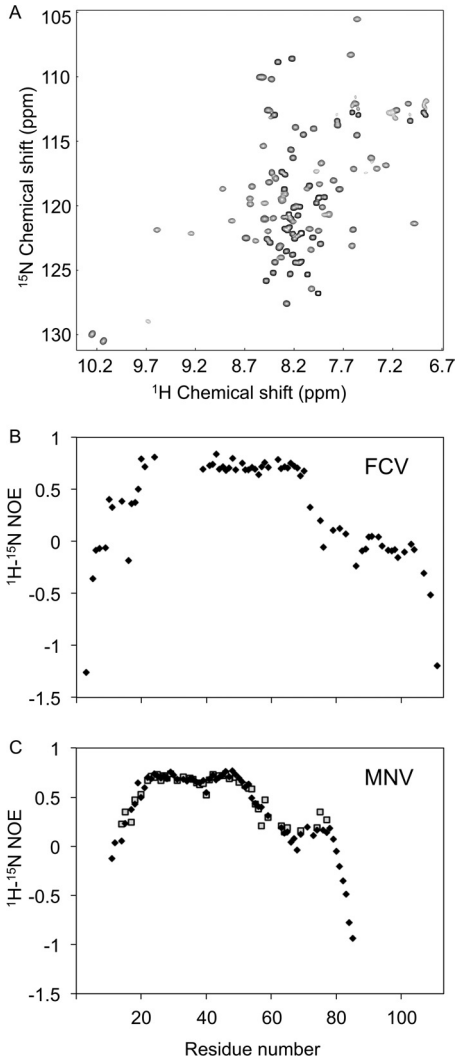


**FIG 1** $^{1}$H-$^{15}$N HSQC and hetNOE data for FCV and MNV VPg proteins. (A) $^{1}$H-$^{15}$N HSQC spectrum for FCV VPg. (B) $^{1}$H-$^{15}$N hetNOE measurements for full-length FCV VPg, plotted against residue number. The gap in the data corresponds to amides from residues 26 to 38 inclusive, which were not able to be assigned from data collected at 298 K. (C) $^{1}$H-$^{15}$N hetNOE measurements for MNV VPg full length (1 to 124) (filled diamonds) and MNV VPg 11-85 (open squares). The backbone amides of residues 1 to 10 and 86 to 124 were not assigned.

MNV VPg 1-124 used in NaCl, pH, and temperature titrations was performed by size exclusion chromatography on an S75 16/60 column (GE Healthcare) with a buffer containing 50 mM sodium phosphate (pH 6.5), 300 mM NaCl, and 1 mM DTT.

FCV VPg 1-111 used in backbone assignments and hetNOE analysis was purified using the same protocol as for MNV VPg 11-82. FCV VPg 9-79 was purified by one-step affinity chromatography to Ni-nitrilotriacetic acid (NTA) agarose resin (Qiagen). MNV VPg 1-124 and FCV VPg 1-111 and mutant proteins for use in 1D NMR were purified by one-step affinity chromatography using Talon resin.

**MNV and FCV VPg assignment and structure determination.** All NMR spectra were recorded on Bruker 500-, 600-, or 800-MHz spectrometers. Backbone assignments of FCV VPg 1-111 were obtained using the following 3D heteronuclear experiments: HNCA, CBCA(CO)NH, HNCACB, HNCO, HN(CA)CO, HBHA(CBCACO)NH, and $^{1}$H-$^{15}$N NOESY (NNOESY) HSQC. Additionally, hetNOE data for FCV VPg 1-111 were recorded. All these experiments were done using FCV VPg at a concentration of 0.5 to 1.0 mM in buffer composed of 50 mM sodium phosphate (pH 6.5), 200 mM NaCl, 1 mM EDTA, 1 mM $NaN_3$, and 1 mM β-mercaptoethanol at 298 K. Data were analyzed using NMRView version 4.1.3 (One Moon Scientific).

For both MNV VPg 11-85 and FCV VPg 9-79, the proteins used in structure determination and backbone and aliphatic side chain assignments were completed using an in-house NMRView-based assignment protocol (58). This was initially used in combination with MARS to establish sequential connectivity, after which assignments were completed (59). The experiments used in the backbone assignment were HNCACB, CBCA(CO)NH, HNCO, and HN(CA)CO. Aliphatic side chain assignment was completed primarily using the HBHA(CBCA)NH, H(C)CH TOCSY, and (H)CCH TOSCY experiments; in addition, the H(CC)(CO)NH and (H)CC(CO)NH TOCSY experiments were used in MNV VPg 11-85 for these assignments. Aromatic side chain assignments were made primarily using NOE correlation of aromatic side groups to the assigned $H_\beta$ and an aromatic $^{1}$H-$^{13}$C HSQC. In addition, (HB)CB-(CGCD)HD and (HB)CB(CGCDCE)HE experiments were used in the MNV VPg 11-85 aromatic assignment. NOE distance restraints were derived using the NNOESY HSQC and $^{1}$H-$^{13}$C NOESY (CNOESY) HMQC experiments. NOESY mixing times for FCV and MNV proteins were 100 ms and 125 ms, respectively. In all structure determination experiments, FCV VPg 9-79 was at a concentration of 100 to 200 μM in 20 mM HEPES (pH 7), 300 mM NaCl, and 1 mM $NaN_3$. MNV VPg 11-85 was at a concentration of 590 μM in 50 mM sodium phosphate (pH 6.5), 300 mM NaCl, and 1 mM DTT for all but the $^{1}$H-$^{13}$C NOESY-HMQC, H(C)CH-TOCSY, (HB)CB-(CGCD)HD, (HB)CB(CGCDCE)HE, and (H)CCH-TOSCY experiments. For these experiments, the protein was at 710 μM in 60 mM sodium phosphate (pH 6.5), 360 mM NaCl, 1 mM DTT, 0.1% (wt/vol) $NaN_3$, and 1× Complete protease inhibitor cocktail (Roche).

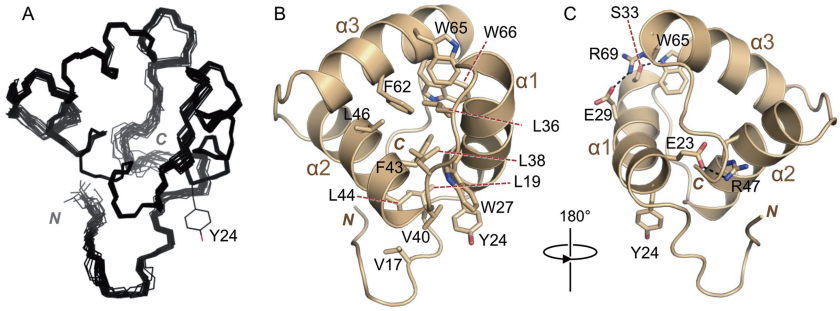


**FIG 2** Solution structure of FCV VPg 9-79. (A) Backbone trace of the 20 lowest-energy conformers of FCV VPg 9-79, calculated using ARIA (62) and CNS (60), including a final water refinement. The nucleotide-accepting tyrosine (Y24) side chain of one of the models is shown. (B) Representative conformer of FCV VPg 9-79, with selected (mainly hydrophobic) side chains shown as sticks and colored by atom type (tan, carbon; red, oxygen; blue, nitrogen). The N and C termini are indicated. (C) FCV VPg 9-79 rotated by 180° compared to panel B and with key charged and polar residues involved in electrostatic interactions shown as sticks. Polar interactions are indicated by dashed black lines.

**TABLE 1** Summary of NMR data and model calculation statistics[a]

| Parameter group and parameter | MNV VPg 11-85 | FCV VPg 9-79 |
|---|---|---|
| Restraints | | |
| Total no. of restraints | 1,248 | 1,335 |
| No. of NOE-derived restraints | 1,176 | 1,172 |
| No. of unambiguous NOE restraints | 618 | 867 |
| No. of ambiguous NOE restraints | 558 | 305 |
| No. of intraresidual NOE restraints ($\|i - j\| = 0$)[d] | 262 | 373 |
| No. of sequential NOE restraints ($\|i - j\| = 1$)[d] | 106 | 197 |
| No. of medium-range NOE restraints ($1 < \|i - j\| \leq 4$)[d] | 140 | 153 |
| No. of long-range NOE restraints ($\|i - j\| > 4$)[d] | 110 | 144 |
| No. of Ψ/Φ dihedral angle restraints | 72 | 84 |
| No. of HN RDC restraints | - | 37 |
| No. of hydrogen bond restraints | - | 42 |
| RMSD from exptl restraints[b] | | |
| Distance (Å) | 0.032 ± 0.001 | 0.057 ± 0.002 |
| Dihedral angle (°) | 0.16 ± 0.07 | 0.755 ± 0.13 |
| NOE/dihedral violations | | |
| No. of NOE violations >0.5 Å | 0 | 0.4 ± 0.5 |
| No. of NOE violations >0.3 Å | 0.60 ± 0.66 | 4.55 ± 1.6 |
| No. of dihedral violations >5° | 0 | 0 |
| RMSD from idealized covalent geometry[b] | | |
| Bond (Å) | 0.0038 ± 0.0001 | 0.0058 ± 0.0002 |
| Angle (°) | 0.48 ± 0.01 | 0.76 ± 0.02 |
| Impropers (°) | 1.15 ± 0.06 | 2.01 ± 0.08 |
| Energies (kcal/mol)[b] | | |
| $E_{total}$ | −2,673.45 ± 86.02 | −2,047.81 ± 71.2 |
| $E_{NOE}$ | 59.98 ± 1.84 | 198.41 ± 15.1 |
| $E_{bond}$ | 17.74 ± 1.38 | 36.61 ± 2.4 |
| $E_{angle}$ | 78.53 ± 4.10 | 165.8 ± 10.9 |
| $E_{vdw}$ | −626.53 ± 6.15 | −655.064 ± 7.0 |
| Coordinate RMSD (Å)[b] | | |
| Backbone atoms in secondary structure | 0.32 ± 0.1 | 0.17 ± 0.03 |
| All heavy atoms in secondary structure | 0.81 ± 0.1 | 0.54 ± 0.1 |
| All backbone atoms | 6.61 ± 1.8 | 0.36 ± 0.1 |
| All heavy atoms | 7.12 ± 1.8 | 0.66 ± 0.1 |
| Ramachandran plot[b,c] | | |
| Most favored (%) | 99.6 | 82.3 |
| Allowed (%) | 0.4 | 14.4 |
| Disallowed (%) | 0 | 3.3 |
| PDB ID | 2M4G | 2M4H |

[a] Structure statistics for MNV VPg 11-85 and FCV VPg 9-79. Averages are given with one standard deviation of the mean.
[b] Determined with an ensemble of the lowest-energy 20 structures which were water refined.
[c] Ramachandran statistics were calculated using MolProbity (65). These were calculated using the core domains of the proteins as determined by MolProbity (MNV VPg 21-55 and FCV VPg 17-73). PDB ID, Protein Data Bank identification number.

Despite buffer differences, the NOESY and side chain experiments, recorded in different buffers, correlate very well with each other. Experiments on MNV VPg 11-85 and FCV VPg 9-79 were recorded at 303 K and 283 K, respectively.

NOEs were assigned and structures were calculated using the ARIA protocol and CNS, including a final water refinement (60–62). TALOS+ was used to generate dihedral angle restraints that were also implemented in the structure calculation (63). In the case of FCV VPg 9-79, $^{1}H$-$^{15}N$ residual dipolar coupling (RDC) restraints were also applied. In-phase/anti-phase (IPAP) $^{1}H$-$^{15}N$ HSQC spectra were recorded under conditions described previously and with 15 mg/ml PF1 filamentous phage as alignment medium (ASLA Biotech). Model validation of FCV and MNV VPg structures was performed using PSVS (64).

**Validation of the MNV VPg structure.** $^{1}H$-$^{15}N$ HSQC spectra of MNV VPg 1-124 and 11-62 for structure validation purposes were recorded at 240 μM and 550 μM protein concentrations, respectively, in 50 mM sodium phosphate (pH 6.5), 300 mM NaCl, and 1 mM DTT. These experiments were performed at 303 K and compared to the reference $^{1}H$-$^{15}N$ HSQC of MNV VPg 11-85 obtained using 590 μM protein in 50 mM sodium phosphate (pH 6.5), 300 mM NaCl, and 1 mM DTT. Heteronuclear NOE experiments were performed using both MNV VPg 11-85 and MNV VPg 1-124 at concentrations of 590 μM and 420 μM, respectively. The buffer conditions were the same as those for the MNV VPg 1-124 $^{1}H$-$^{15}N$ HSQC, with the exception that 0.1% $NaN_3$ and 1× Complete protease inhibitor cocktail were present in the VPg 11-85 sample.

**1D NMR of VPg mutants.** The 1D NMR spectra of wild-type (WT) and mutant MNV VPg 1-124 proteins were typically recorded at 298 K in 50 mM Tris (pH 7), 300 mM NaCl, and 2 mM β-mercaptoethanol. These conditions were also used for FCV VPg 1-111 and mutants thereof, with the exception that 150 mM NaCl was used. The protein concentration used was ~45 μM for FCV VPg and between 90 and 170 μM for MNV VPg.

**MNV and FCV viability assays.** For FCV, the QuikChange II XL site-directed mutagenesis kit (Agilent Technologies, Inc.) and set of mutagenic primers were used to modify the FCV full-length cDNA clone pQ14 (8) to introduce amino acid changes into the FCV VPg sequence at positions 30 (H to A, I), 43 (F to A), 47 (R to E, G), 62 (F to A), 65 (W to A), 66 (W to A), and 69 (R to E). The modified clones were screened by sequencing, and plasmids containing desired mutations were selected for further experiments. The recovery of infectious FCV from the selected full-length cDNA clones was conducted using capped *in vitro*-transcribed RNA as described previously (8, 65) but with the minor modification of using enzymatically capped RNA transcripts as described previously (11). CRFK (Crandell-Rees feline kidney) cells were transfected with capped genomic RNA transcripts synthesized from the corresponding plasmid DNA templates by *in vitro* transcription using T7 RNA polymerase. Cells were transfected with 1 μg of RNA using Lipofectamine 2000 (Invitrogen) and incubated at 37°C for 24 h. Cells were freeze-thawed at −80°C to release virus particles, and viral titer was determined using the 50% tissue culture infective dose ($TCID_{50}$) on CRFK cells.

For MNV, mutations in VPg were introduced by overlapping PCR mutagenesis, with the mutagenized region being inserted back into the MNV-1 full-length infectious clone pT7:MNV 3′Rz. The complete sequence of the mutagenized region was determined in all cases prior to use. The effect of the various VPg mutations on virus recovery was determined using the reverse genetics system based on recombinant Fowlpox expressing T7 RNA polymerase as previously described (7). Briefly, BSRT7 cells were infected with fowlpox virus expressing T7 RNA polymerase (based on the virus titer in chicken embryo fibroblasts) at a multiplicity of infection (MOI) of 0.5 PFU per cell. After 2 h, 1 μg of each MNV cDNA construct was transfected using Lipofectamine 2000 according to the manufacturer's instructions. At 24 h after transfection of DNA, the cells were freeze-thawed at −80°C to release virus particles and the viral titer was determined using the $TCID_{50}$ on RAW264.7 cells. In all cases, the expression of the viral RNA polymerase NS7 24 h after transfection of the cDNA construct was analyzed by Western blot to confirm equal transfection efficiency.

**VPg-RNA synthesis assays.** The MNV RdRp and VPg coding regions were amplified using PCR from the MNV-1 infectious clone pT7:MNV 3′Rz (GenBank accession number DQ285629.1) and cloned into the pUNO vector (InvivoGen, San Diego, CA). All VPg mutants were generated using specific forward and reverse primers and the QuikChange mutagenesis kit (Agilent Technologies). All plasmid constructs were confirmed by DNA sequencing using the BigDye Terminator v3.1 cycle sequencing kit (Applied Biosystems).

The norovirus (NoV)-5BR assay was used to determine the efficiency of RNA synthesis (45). In this assay, HEK293T cells were transiently transfected with plasmids to express the NoV RdRp and the components needed to detect the RNAs produced by the NoV polymerase and, where appropriate, with VPg. The RNAs synthesized by the NoV RdRp activate signal transduction by the innate immune receptor RIG-I, which leads to expression of the firefly luciferase reporter that is under the control of the beta interferon (IFN-β) promoter. The cells also express the *Renilla* luciferase under the control of a constitutive promoter to monitor transfection efficiency and cytotoxicity. Briefly, $1 \times 10^5$ HEK293T cells were seeded in a Costar 96-well plate with Dulbecco's modified Eagle medium (DMEM) and 10% fetal bovine serum for 24 h prior to cotransfection of the plasmids that can express VPg, $NS7^{pol}$, RIG-I, and the two reporter luciferases. At 36 h posttransfection, luciferase levels were determined using the Dual-Glo luciferase assay system (Promega) and a Synergy 2 microtiter plate reader (BioTek). RNA synthesis efficiency is reported as the ratio of firefly to *Renilla* luciferase activities.

A VPg-RNA electrophoretic mobility shift assay (EMSA) was used to determine whether the NoV RdRp used VPg as a protein primer for RNA synthesis. HEK293T cells ($1.0 \times 10^6$/ml in 6-well plates [BD Falcon]) were transfected with hemagglutinin (HA)-tagged WT or mutant MNV VPgs along with FLAG-tagged $NS7^{pol}$ 24 h posttransfection. VPg and VPg-RNA were immunoprecipitated using anti-HA polyclonal antibody covalently linked to Dynabeads M-270 epoxy resin, resolved on a 4 to 12% NuPAGE Novex Bis-Tris gel and morpholinepropanesulfonic acid-SDS running buffer

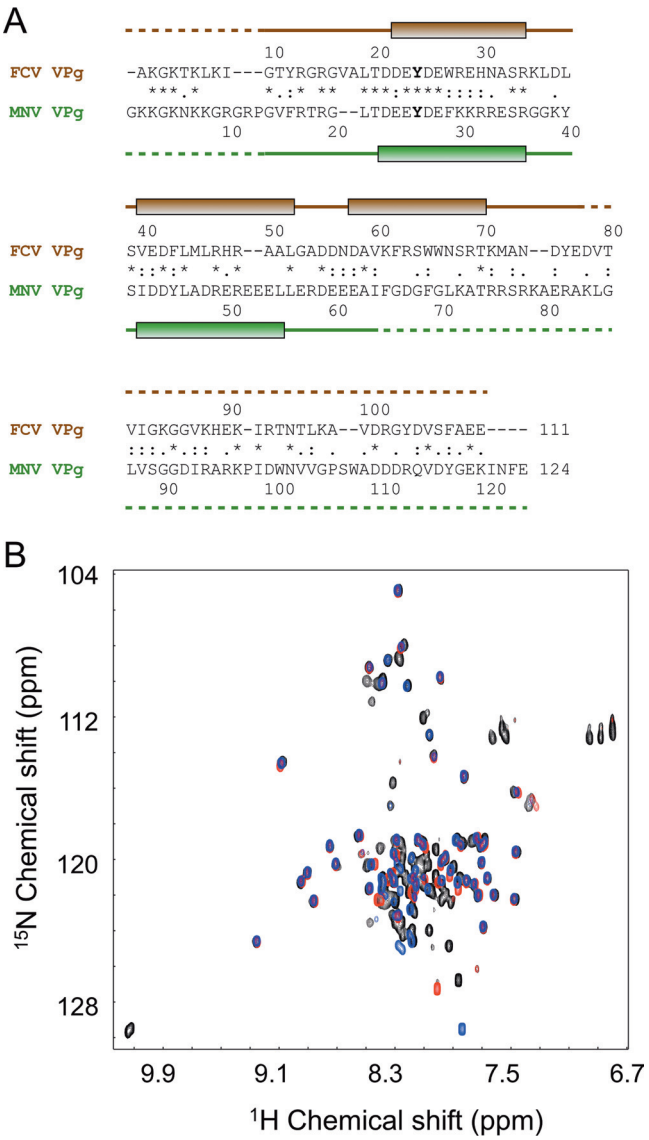


**FIG 3** NMR analysis of the MNV VPg benefitted from knowledge of the structure of FCV VPg. (A) Amino acid sequence alignment of FCV and MNV VPg proteins, performed using ClustalW. Positions of the helices detected through structural analysis are indicated as shaded boxes above and below the sequences (green for FCV and brown for MNV). Dashed lines indicate disordered portions of the polypeptide backbone. The nucleotidylated Tyr in each sequence is shown in boldface. Within the alignment, the asterisk, colon, and period characters denote identical, very similar, and similar amino acids, respectively. (B) Overlay of $^{1}$H-$^{15}$N HQSC spectra of MNV VPg constructs used to probe the extent of the structure core of the protein: blue, VPg 11-85; black, VPg 1-124; red, VPg 11-62.

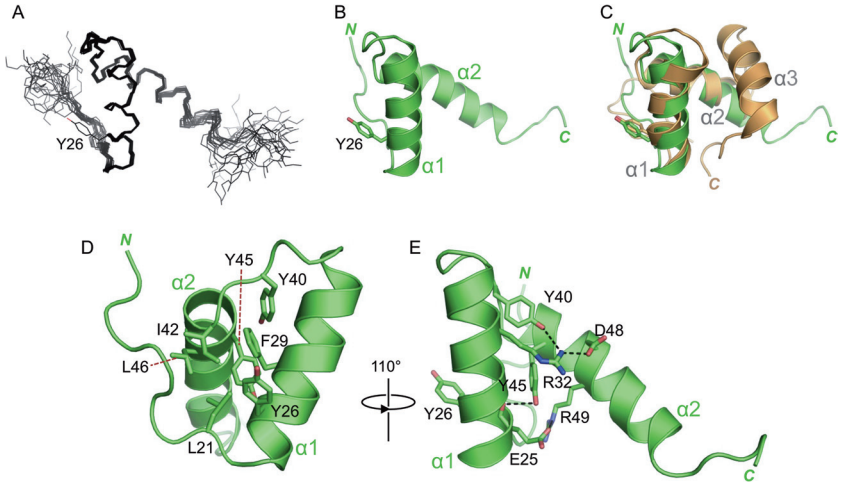


**FIG 4** Solution structure of MNV VPg 11-85. (A) Backbone trace of the 20 lowest-energy conformers of MNV VPg 11-85, calculated by ARIA (62) and CNS (60). The side chain of the nucleotide-accepting tyrosine from one of the conformers is indicated. (B) Representative conformer of MNV VPg 11-85. The N and C termini are indicated. (C) Overlay of the structured cores of FCV VPg (tan) and MNV VPg (green); the backbone RMSD between the two structures is ~2 Å. (D) Representative conformer of MNV VPg 11-85, with selected (mainly hydrophobic) side chains shown as sticks and colored by atom type. (E) MNV VPg 11-85 rotated by 110° compared to panel D and with key charged and polar residues involved in electrostatic interactions shown as sticks. Polar interactions are indicated by dashed black lines.

(Invitrogen), and transferred to a polyvinylidene fluoride (PVDF) membrane, which was then probed with anti-HA antibodies to detect VPg (45).

**Protein structure accession numbers.** Coordinates and NMR data have been deposited with the Protein Data Bank. The accession numbers are 2M4G (MNV VPg 11-85) and 2M4H (FCV VPg 9-79).

## RESULTS

**Solution structure of FCV VPg.** Given previous reports of the intrinsically disordered nature of VPg proteins, we sought first to determine whether FCV VPg contained structured regions by analyzing a $^{1}$H-$^{15}$N HSQC spectrum. The dispersion of amide peaks evident in the spectrum recorded for full-length FCV VPg (residues 1 to 111) indicated that the protein was at least partially structured (Fig. 1A). To define the structured portions of the protein, peaks in the spectrum corresponding to backbone amides were assigned (see Materials and Methods). Backbone amide assignments were made for 98 of the 111 residues; curiously, the 13 peaks missing from the spectrum corresponded to a contiguous portion—residues 26 to 38—of the VPg sequence.

$^{1}$H-$^{15}$N hetNOE measurements were used to determine the dynamics of each backbone amide group on a picosecond-to-nanosecond time scale. The assigned amides for residues 12 to 72 had hetNOE values greater than 0.5, indicative of a structured domain (Fig. 1B). Outside this region, hetNOE values were close to or less than zero, revealing that the N-terminal 11 residues and the C-terminal 39 residues of the protein are more mobile. FCV VPg thus appears to possess a structured core flanked by flexible termini. As a result of these initial characterizations, a construct that expressed FCV VPg 9-79 was generated for solution structure determination.

A protein containing residues 9 to 79 of the FCV VPg was analyzed by $^{1}$H-$^{15}$N HSQC at 298 K and was also found to lack signals corresponding to backbone amides for residues 26 to 38. The absence of peaks associated with this region of the protein is likely due to local conformational exchange at millisecond-to-microsecond time scales. To attempt to move these dynamics out of the intermediate exchange regime, we recorded NMR data at reduced temperatures (down to 278 K). Under these conditions, additional peaks that permitted the assignment of all the missing residues from 26 to 38 apart from R34 were observed in $^{1}$H-$^{15}$N HSQC spectra. All subsequent NMR analyses of FCV VPg 9-79 were performed at 283 K (see Materials and Methods); although the lower temperature reduced the signal-to-noise ratio in these experiments, a reliable structure of FCV VPg 9-79 was obtained. The 20 final water-refined conformers with the lowest energy have a backbone root mean square deviation (RMSD) of 0.17 Å (Fig. 2A). Structure determination statistics are given in Table 1.

This structural analysis of FCV VPg 9-79 revealed a compact core domain (residues 14 to 76) that is largely composed of a three-helix bundle (Fig. 2B and C). Residues 22 to 34, 40 to 52, and 57 to 70 make up helices α1, α2, and α3, respectively, and are connected by short loops that allow α2 and α3 to each pack at approximately right angles to the preceding helix. The tightly packed helical bundle at the core of FCV VPg is stabilized by an extensive hydrophobic core consisting of residues V17, L19, W27, L36, L38, V40, F43, L44, L46, F62, W65, and W66 (Fig. 2B). Residues 10 to 19 at the N-terminal end of the core form a tight turn that packs against helix α2.

**Determination of the solution structure of MNV VPg.** The FCV and MNV VPg proteins used in this work share 27% identity overall and 40% identity in their N-terminal halves (37) (Fig. 3A). The relatively high level of sequence similarity between them and the structural insights from the FCV VPg led us to design an MNV VPg 11-85 construct that was predicted to correspond to the structured core of the FCV VPg (Fig. 3A).

The $^{1}$H-$^{15}$N HSQC spectrum of MNV VPg 11-85 exhibited good dispersion (Fig. 3B), indicative of a defined structure, but did not have the conformational exchange issues encountered with FCV VPg. Therefore, the sample was analyzed at 303 K to optimize the signal-to-noise ratio. A good-quality structure was obtained for MNV VPg 11-85, which had a backbone RMSD of 0.32 Å for the ordered residues in the 20 lowest-energy structures (residues 21 to 55 inclusive) (Fig. 4A). Full structure determination statistics are in Table 1.

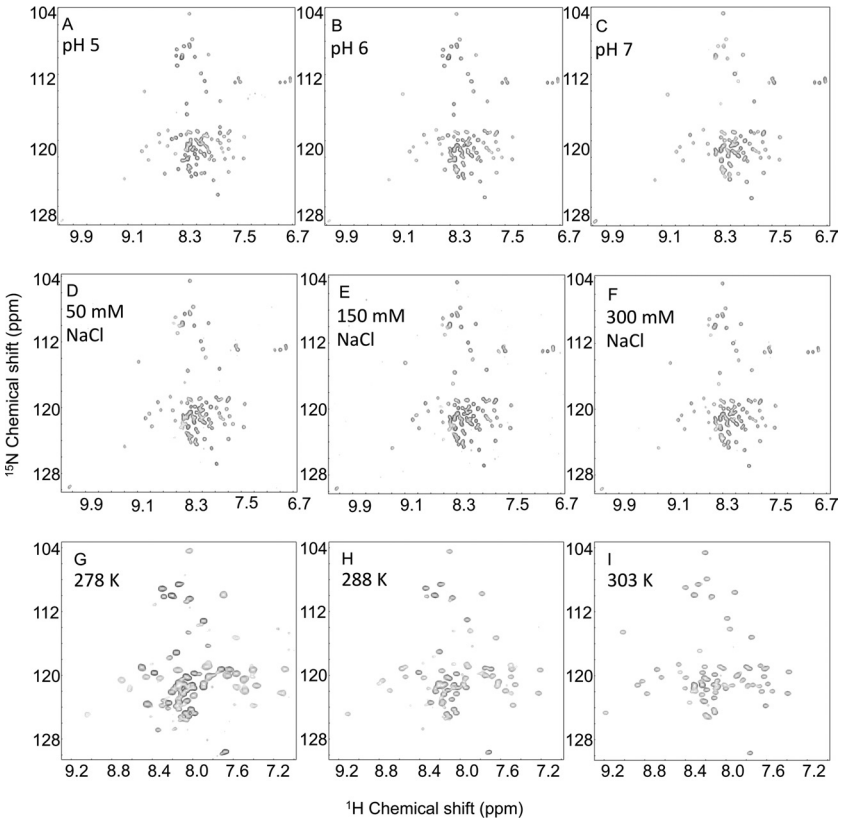


**FIG 5** Effects of pH, NaCl, and temperature on the $^{1}$H-$^{15}$N HSQC spectrum of MNV VPg 1-124. (A to C) Spectra recorded for MNV VPg 1-124 at pH 5 (A), pH 6 (B), or pH 7 (C). The spectra were recorded at 303 K with 100 μM protein dissolved in 50 mM malic acid, 2-(N-morpholino)ethanesulfonic acid (MES), and Tris-HCl at a molar ratio of 1:2:2 (MMT), 300 mM NaCl, and 1 mM DTT, which was titrated to the required pH with HCl or NaOH as appropriate. (D to F) $^{1}$H-$^{15}$N HSQC spectra recorded at 303 K with 40 μM protein in 50 mM sodium phosphate (pH 6.5) and 1 mM DTT supplemented with 50 mM NaCl (D), 150 mM NaCl (E), or 300 mM NaCl (F). (G to I) $^{1}$H-$^{15}$N HSQC spectra recorded with 590 μM protein in 50 mM sodium phosphate (pH 6.5), 300 mM NaCl, and 1 mM DTT at 278 K (G), 293 K (H), or 303 K (I).

Strikingly, the MNV VPg core domain contains only two helices, formed by residues 23 to 35 and 42 to 55 (Fig. 4B). These overlay well with the first two helices in the FCV VPg structure (backbone RMSD, 2.0 Å) (Fig. 4C). The third helix observed in the FCV core structure is absent from MNV VPg 11-85; instead, residues 56 to 85 of the MNV VPg adopt an extended conformation that varies in position in all of the final conformers.

**Validation of the two-helix model of the MNV VPg core.** The absence of the third helix in the core of MNV VPg was unexpected, particularly since the MNV VPg protein is significantly larger than that of FCV VPg. To confirm the absence of this helix, we compared $^{1}$H-$^{15}$N HSQC spectra of MNV VPg 11-85 with those obtained from MNV VPg 1-124 (full length) and MNV VPg 11-62, the latter being a construct truncated to contain just the two-helix core. The amide signals from the core two-helix domains of all three proteins were found to overlay closely (Fig. 3B). Moreover, in comparison to the spectrum for MNV VPg 11-62, there were no additional backbone $^{1}$H-$^{15}$N signals outside the center of the spectrum (in the proton dimension) observed for MNV VPg 1-124. These observations are consistent with the two-helix structure for MNV VPg.

Further support for the observed structure is found in the hetNOE data for MNV VPg 1-124 and VPg 11-85, which show that helices α1 and α2 in MNV VPg are rigid: the hetNOE values of this region of ~0.65 to 0.8 strongly indicate that the two helices have a stable tertiary structure (Fig. 1C). In contrast, the region that aligns to helix α3 of FCV VPg has much lower hetNOE values (~0.2), indicative of significantly greater mobility than the preceding two helices. It is possible that residues in the MNV VPg corresponding to helix α3 of the FCV VPg have a residual structural propensity that was not captured under our NMR conditions. To test this notion, $^{1}$H-$^{15}$N HSQC spectra were recorded over a range of pH values, NaCl concentrations, and temperatures to probe their effects on the structure of the protein. MNV VPg 1-124 spectra recorded at pH 4, 5, 6, 7, and 8 showed that although the protein appears to be unfolded at pH 4, in the pH range of 5 to 8, there are no significant changes in the spectra, consistent with a stable structure (Fig. 5A to C). Similarly, $^{1}$H-$^{15}$N HSQC spectra recorded from MNV VPg 1-124 in buffer containing 50, 150, or 300 mM NaCl (pH 6.5) were almost identical (Fig. 5D to F). Finally, no significant changes in $^{1}$H-$^{15}$N spectra were recorded from MNV VPg 11-85 at 278 K, 283 K, 288 K, 293 K, 298 K, or 303 K; the only notable spectral changes were due to the well-documented temperature dependence of the amide $^{1}$H chemical shift (66). The close similarity of spectra recorded at 278, 288, and 303 K (Fig. 5G to I) strongly suggests that the structure of MNV VPg 11-85 does not significantly change over this temperature range. We conclude that the absence of helix α3 from MNV VPg is unlikely to be an artifact of the conditions under which NOESY experiments were recorded.

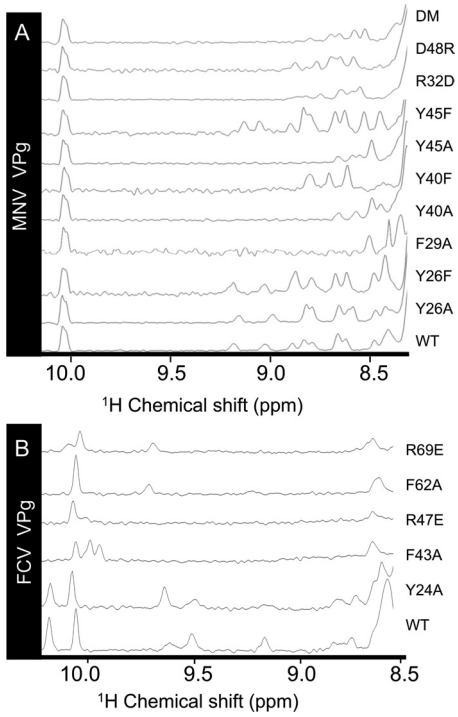


**FIG 6** Effects of site-directed mutations on the stability of the core structures of MNV and FCV VPg. The amide region of the 1D $^1$H NMR spectra of MNV VPg 1-124 (A) and FCV VPg 1-111 (B). In each case, the region of the spectrum shown is the structured amide region of a 1D protein spectrum, which is not overlapped by aromatic signals. The peaks at 10.0 to 10.3 ppm derive from the $NH^{\varepsilon}$ of Trp side chains.

**Correlating VPg structure to function.** The nucleotide acceptors of FCV and MNV VPg proteins, Y24 and Y26, respectively (44, 45), are located toward the N-terminal end of helix α1 in both molecules (Fig. 4C). This observation raises the question of how VPg interacts with the polymerase to mediate the nucleotidylation reaction because the structured core of VPg (approximately 20 Å by 20 Å by 30 Å for MNV) appears too large to fit within the enclosed substrate-binding channel in the calicivirus NS7 polymerase, which has a minimum dimension of about 12 Å (21, 67–69). It seems likely, therefore, that either VPg or $NS7^{pol}$ (or both) undergoes a significant conformational change in order to form a complex that is competent for nucleotidylation.

To probe whether some relaxation of the VPg structure might be necessary for its function, we introduced destabilizing mutations into VPg and examined their effect on the folded state and activity of the protein. In the first phase of these experiments, we determined the destabilizing effects of mutation in full-length MNV VPg using 1D $^1$H NMR. Mutants F29A, Y40A, and Y45A were found to be severely destabilized, as indicated by disappearance of almost all the structured amide signals from the NMR spectrum (Fig. 6A). The structurally more conservative mutation Y40F restored some but not all of the missing amide peaks, indicative of a lesser degree of destabilization than with the alanine substitution. In the case of the Y45F mutation, the spectrum is very similar to that of the wild-type protein. The greater disruption observed for Y40F may be attributable to the role of the Y40 hydroxyl group in stabilizing the guanidinium group of R32 in wild-type MNV VPg (Fig. 4E). In contrast to the effects of nonconservative mutation of buried Tyr residues, substitution by alanine of the solvent-exposed side chain of Y26 (the nucleotide acceptor) did not significantly affect the structured amide signals visible in the 1D $^1$H NMR spectrum.

We also probed the ability of charged residues observed to be involved in electrostatic interactions to affect the stability of the MNV VPg core. Mutants R32D and D48R that should contain a disrupted interhelical salt bridge (Fig. 4E) had fewer structured amides in the NMR spectrum but appeared to retain some residual core structure (Fig. 6A). An attempt to restore this salt bridge using an R32D D48R double mutant did not stabilize the VPg core. This is perhaps not surprising given that R32 is also stabilized by interaction with the hydroxyl of Y40 (Fig. 4E).

For FCV VPg, F43A and F62A mutations were introduced to destabilize the hydrophobic core while R47E and R69E were introduced to disrupt electrostatic interactions between helix α1 and helix α2 and between helix α1 and helix α3, respectively. The structured amide region of the wild-type FCV 1-111 spectrum has only 5 amide peaks as markers of structure, but the spectra of the F43A and R47E mutants lacked these peaks, indicative of a large disruption to the protein structure (Fig. 6B). F62A and R69E retain only one of these peaks, suggestive of a core with some residual structure. As with MNV VPg, mutation of the nucleotide-accepting tyrosine Y24 provided a useful negative control: the Y24A substitution resulted in a spectrum that is very similar to that of wild-type FCV VPg.

Having examined their effects on VPg stability, we next sought to determine whether these mutations affected the ability of MNV VPg to interact with the RdRp and to be nucleotidylated. At the same time, we also aimed to define in greater detail the regions in the MNV VPg needed for functional interaction with the viral polymerase. In the absence of an *in vitro* nucleotidylation assay for FCV or MNV VPg that recapitulates the specificity observed during infection (70), the functional VPg-RdRp interaction was monitored using a transient-transfection assay that detects MNV polymerase activity (45). In this assay, the RNAs synthesized by the MNV RdRp serve as agonists for the innate immune receptor RIG-I, activation of which leads to firefly luciferase reporter expression from a beta interferon promoter (45). Importantly, coexpression of the wild-type MNV VPg with the MNV polymerase was found to increase luciferase production by about 40 to 50% (71).

An extensive panel of MNV VPg mutations was tested in the assay, with an emphasis on residues located in the core (Fig. 7). Mutations in the unstructured N (K3A, K5A, K7A) and C (V115A, D116A, Y117F) termini did not significantly impair the ability of VPg to enhance RNA synthesis. In contrast, substitution of amino acids within the highly conserved $^{21}$LTDEEYDE$^{28}$ motif that contains the nucleotide acceptor (Y26) (Fig. 3A) reduced the ability of the VPg to stimulate RdRp activity (see the bar graph in Fig. 7).

Mutation of Y40 and Y45, residues that contribute to the stability of the core, had variable effects (Fig. 7). Although Y40A and Y45A are both largely destabilizing, VPg containing Y40A was not able to synthesize VPg-RNA and did not stimulate RNA synthesis, while Y45A was associated with an intermediate level of activity (Fig. 7). Intriguingly, mutant Y40F, which is more stable than Y40A, had close to wild-type activity for VPg-enhanced RNA synthesis and for the production of the VPg-RNA, whereas introduction of Y45F, which does not significantly perturb the core structure (Fig. 6A), surprisingly rendered VPg defective for these

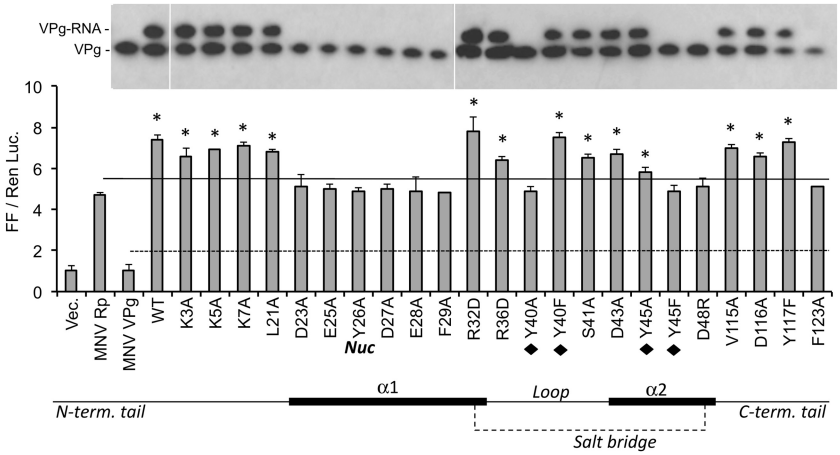


**FIG 7** Effects of mutations on MNV VPg on RNA synthesis by MNV NS7$^{Pol}$. The bar graph shows results from the cell-based reporter assay detecting NS7$^{Pol}$ products by the RIG-I innate immune receptor. Each bar contains the results from 3 independent transfected HEK293T cells, and the results are expressed as a ratio of the firefly (FF) luciferase driven by the IFN-β promoter to a constitutive *Renilla* luciferase (Ren Luc) that was coexpressed within the same cells. Within the bar graph, the solid line represents reporter levels from the NS7$^{Pol}$ in the absence of coexpressed VPg. The dashed line denotes the background reporter levels in the absence of RNA synthesis by the NS7$^{Pol}$. Bars identified with asterisks denote results that are statistically different ($P < 0.05$) from those of the polymerase alone. Under the graph is a schematic representation of key features within the MNV VPg molecule. The thick lines represent the two α-helices in the core, and the bold "Nuc" denotes the location of the nucleotidylation tyrosine. The tyrosines that form a hydrophobic region within the core are identified by black diamonds. The salt bridge between residues R32 and D48 is indicated by a dashed line. The gel images above the graph are from Western blots of immunoprecipitated VPg in cultures tested in parallel to the reporter assay. The identities of VPg and the fractions of the VPg molecules used by the NS7$^{Pol}$ for RNA synthesis are shown to the left of the images. All samples were from one experiment but cropped to allow alignment of the Western blot results to those of the reporter assay.

activities. Finally, although the mutants R32D and D48R should both lack the salt bridge between α-helices, R32D had wild-type activity in the two assays while the D48R mutant was completely inactive (Fig. 7). The effect of the R32D D48R double mutation was not able to be determined since the resultant protein was not expressed in transfected cells (data not shown).

A defect in the ability of MNV VPg to interact with the polymerase should result in decreased production of RNA synthesized using VPg as a primer. To examine whether this was the case, an electrophoretic mobility shift assay was performed using immunoprecipitation of the VPg protein and subsequent detection of VPg and VPg-linked RNA via Western blotting (45, 71). Previous work had shown that the generation of VPg-linked RNA is critically dependent on the addition of RNA and VPg and the presence of the MNV RdRp (45). Consistent with the effect on RNA synthesis by the RdRp, the VPg mutants D23A, E25A, Y26A, Y26F, D27A, F29A, Y40A, Y45F, and D48R were all defective for production of VPg-RNA (Fig. 7). Overall, these results show that a large number of changes in the core of the MNV VPg prevented proper activity. However, mutations that destabilized the core protein *in vitro* did not always abolish VPg activity (e.g., R32D, Y40F) (Table 2).

**Effect of destabilizing mutations in VPg on FCV and MNV infectivity.** In an effort to shed further light on the significance of the structured core within VPg, we also introduced destabilizing mutations into the virus genome using reverse genetics (see Materials and Methods). For MNV, live virus was not able to be recovered from cDNA clones carrying the Y40A or Y45A mutant in VPg, both of which significantly destabilize the protein core (Table 2). However, mutations associated with lesser destabilization gave variable virus yields. For example, although the Y45F mutation is less destabilizing than the Y40F mutation, transcripts containing the Y45F substitution yielded no virus whereas wild-type levels of virus were recovered from cDNA clones carrying the Y40F mutation, a result that parallels the findings from the activity assays (Fig. 7). The partially destabilizing R32D and D48R VPg mutations and the R32D D48R double mutation all produced live virus. In the case of D48R, the yield of the recovered virus was similar to that of the wild type (although notably, this mutation eliminated nucleotidylation activity in cell-based assays) (Fig. 7), while for the R32D and R32D D48R mutants, the recovered virus had a 10-fold-lower yield 24 h posttransfection (Table 2). Oddly, the levels of viral infectivity recovered for R32D and D48R are inversely correlated with the effects of these mutations on the ability of MNV VPg to enhance polymerase activity in our assay (Fig. 7).

In contrast to the results obtained with MNV, no live virus was recovered from the FCV reverse genetics system for any of the VPg destabilization mutations tested (F43A, R47E, F62A, and R69E) (Table 3). This suggests that the FCV core domain may play a more integral role in the FCV life cycle than its MNV counterpart. However, the possibility that some or all of these FCV VPg residues have functions in virus replication that are independent of the stability of the VPg core structure cannot yet be excluded.

## DISCUSSION

In this paper, we report the first high-resolution structural analysis of calicivirus VPg proteins. These structures are surprising in several ways. We find that the VPg proteins of FCV and MNV contain α-helical cores flanked by long unstructured termini, in contrast to the intrinsically disordered nature of smaller picornavirus VPg (49) and the larger VPg proteins from RNA viruses of plants, such as potyvirus (52, 54). Although there is some evidence (from circular dichroism measurements, protease sensitivity assays, and NMR analyses) for the presence of a compact domain within potyvirus VPg, a defined tertiary structure has not been

**TABLE 2** Effect of mutations in the MNV VPg on infectivity, activities, and stability

| Mutation | Virus recovery[a] | NS7$^{pol}$ enhancement[b] | VPg nucleotidylation[c] | VPg core stability[d] |
|---|---|---|---|---|
| Wild type | +++ | + | + | + |
| N-terminal tail | | | | |
| K3A | − | + | + | ND |
| K5A | ++ | + | + | ND |
| K7A | ++ | + | + | ND |
| L21A | − | + | + | ND |
| α-helix 1 | | | | |
| D23A | − | − | − | ND |
| E25A | − | − | − | ND |
| Y26A/F[e] | − | − | − | + |
| D27A | + | − | − | ND |
| E28A | − | − | − | ND |
| F29A | − | − | − | − |
| R32D | ++ | + | + | +/− |
| Loop | | | | |
| R36D | ++ | + | + | ND |
| Y40A | − | − | − | − |
| Y40F | +++ | + | + | +/− |
| S41A | +++ | + | + | ND |
| α-helix 2 | | | | |
| D43A | +++ | + | + | ND |
| Y45A | − | +/− | + | − |
| Y45F | − | − | − | + |
| D48R | +++ | − | − | +/− |
| R32D/D48R | ++ | ND | ND | +/− |
| C-terminal tail | | | | |
| V115A | ++ | + | + | ND |
| D116A | ++ | + | + | ND |
| Y117F | +++ | + | + | ND |

[a] Recovery is expressed as the yield posttransfection relative to that of the wild type (+++) as assayed by >3 independent experiments. Typical yields of wild-type virus were $1 \times 10^4$ to $5 \times 10^4$ $TCID_{50}$ units. −, no virus detected; +, up to 100 $TCID_{50}$ detected; ++, up to 1,000 $TCID_{50}$ detected; +++, up to WT levels of virus detected.
[b] Enhancement of RNA synthesis by NS7$^{pol}$ in the luciferase reporter assay is denoted as a plus (+) when the luciferase reporters are statistically above the signal from NS7$^{pol}$ expressed without VPg at a *P* value of >0.05 in the Student *t* test.
[c] VPg nucleotidylation is derived from the Western blots in Fig. 7.
[d] VPg core stability was assessed from $^1$H NMR shift data in Fig. 6A. The WT VPg core contains nine distinct peaks, and samples with 8 or more peaks are denoted with a +. Samples with three to five peaks are denoted with a +/−, and samples with less than three peaks are denoted with a −. ND, not determined.
[e] Infectivity data are for Y26F; other assay data are for Y26A.

**TABLE 3** Effect of mutations in FCV VPg on virus infectivity

| VPg mutation | Virus recovery[a] |
|---|---|
| Wild type | +++ |
| H30I | ++ |
| H30A | + |
| F43A | − |
| R47E | − |
| R47G | − |
| F62A | − |
| W65A | − |
| W66A | − |
| R69E | − |

[a] Recovery is expressed as the yield 24 h posttransfection relative to that of the wild type (+++) as assayed by >3 independent experiments. Typical yields of wild-type virus were $1 \times 10^4$ to $5 \times 10^4$ $TCID_{50}$ units. −, no virus detected; +, up to 100 $TCID_{50}$ detected; ++, up to 1,000 $TCID_{50}$ detected; +++, up to WT levels of virus detected.

detected; rather, the core within this protein appears to have the properties of a dynamic molten globule (54).

These new observations for calicivirus VPg proteins emphasize the structural diversity within this broad grouping of VPg proteins, which likely also reflects their different functions. While the VPgs of picornaviruses, caliciviruses, and potyviruses all have a role in viral replication by serving as a protein primer for the initiation of RNA synthesis, their additional functions vary (55, 72). Calicivirus VPgs are known to be critical for the initiation of viral protein synthesis (25) by recruiting host cell initiation factors to the viral RNA (35–37). In contrast, the short ~22-amino-acid VPg from picornaviruses is not involved in translation initiation; instead, this function is assumed by an elaborate RNA structure, the internal ribosome entry site (IRES), within the 5′ untranslated region of the viral genome (72). Potyvirus VPg is different again; although the potyvirus RNA genome also contains an IRES that is required for translation initiation (55), its VPg protein makes an interaction with the eukaryotic initiation factor eIF4E that is critical for infection (39, 41). However, it is not yet clear whether this interaction is needed to initiate translation; it may alternatively serve to suppress host-cell protein synthesis (73). More-recent data have revealed interactions between potyvirus VPg (or its precursors) and other components of the translation initiation machinery, such as PABP, eIF4G, and eIF4A, that may be functionally important (reviewed in reference 55).

There are clear differences between the VPg structures for MNV and FCV. While the VPg core from the vesivirus FCV has a three-helix bundle, the murine norovirus VPg core contains just the first two helices of this structure (Fig. 2 and 4). Strikingly, despite significant structural variation, the hydrophobic core residues in helix α1 and helix α2 of FCV VPg are largely conserved in the MNV structure: residues L21, F29, Y40, I42, Y45, and L46 of MNV VPg overlay closely with L19, W27, L38, V40, F43, and L44 of FCV VPg, respectively (Fig. 4C and D). Given that FCV and MNV are representative members of the two major clades that caliciviruses can be divided into on the basis of VPg nucleotide sequences (74), the structures reported should serve as useful models for other calicivirus VPg proteins; in particular, helices α1 and α2 are likely to be conserved features.

Aside from the helix content, one of the most notable differences between FCV and MNV VPg occurs within the sequence of helix 2. In FCV VPg, the helix α2 sequence $^{40}$VEDFLMLRHRA AL$^{52}$ is replaced in the MNV protein by $^{42}$IDDYLADREREEELL$^{56}$ (Fig. 3A), which contains many more charged residues. Whereas in FCV VPg, hydrophobic residues on one flank of this helix, notably L46 and A50, make apolar contacts with helix α3, the equivalent residues in MNV VPg (D48 and E52) are polar and contribute instead to electrostatic stabilization between helices α2 and α1 (Fig. 4E).

An important common feature of calicivirus VPg proteins is the conserved acid-rich motif (E/DEYDEΩ, where Ω denotes F, Y, or W) that contains the Tyr residue nucleotidylated by the viral NS7 polymerase to form primers for RNA synthesis (72). Our results for FCV and MNV VPg reveal that this motif is found in a conserved location, embedded within the first helix of the struc-

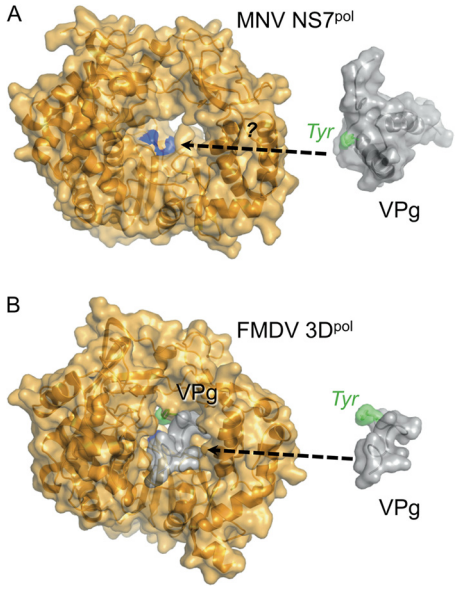


**FIG 8** How does MNV VPg interact with its polymerase? Comparison of the structures of polymerases and VPg proteins from MNV and FMDV. (A) Crystal structure of MNV NS7$^{pol}$ (67) and solution structure of MNV VPg 11-85 (this work). The active site of the polymerase, where nucleotidylation takes place, is colored blue. It is not yet clear what conformational changes are required for MNV VPg to be accommodated within the active site. (B) Cocrystal structure of FMDV 3D$^{pol}$ and VPg (75), with VPg also shown extracted from the structure on the right (for ease of comparison with panel A). Only residues 1 to 15 of FMDV VPg were visible in the crystal structure.

ture core such that the Tyr side chain points away from the core (Fig. 4C). Remarkably, despite this exposed position, modeling studies suggest that the structure of the core would prevent the Tyr from binding close enough to the active site of NS7$^{pol}$ to be nucleotidylated by the enzyme (Fig. 8).

To probe how the observed structure relates to function, we examined the effects of VPg mutations on MNV infectivity and on the VPg-NS7$^{pol}$ interaction using both a cell-based assay that reported the VPg-mediated stimulation of polymerase activity and an EMSA to monitor the production of VPg-RNA (45, 71). Some care needs to be taken in the comparison of results from these assays because of the significant differences in their methodologies. First, it is important to appreciate that the two assays have very different dynamic ranges. The infectivity assay can detect differences in MNV plaque formation over several logs, while the two assays for VPg-NS7$^{pol}$ interaction have a range of only a few fold. Second, the modulatory effects of VPg on RNA synthesis in the reporter assay rely on RIG-I detection of RNA synthesized by NS7$^{pol}$, followed by signal transduction leading to the activation of the IFN-β promoter. Thus, the readout is an indirect assessment of RNA synthesis by NS7$^{pol}$ and the NS7$^{pol}$-VPg interaction.

However, even with these caveats in mind, we believe that results from these assays are relevant for understanding how VPg structure impacts the functions of the protein. It is notable that the majority of the results from the infectivity assay agreed with those from the interaction assays: mutations that impaired the functional interaction of VPg with NS7$^{pol}$ generally abrogated infectivity (Table 2). Exceptionally, within the VPg N-terminal tail, mutants K3A and L21A retained interaction with NS7$^{pol}$ but were not infectious in the context of the MNV replicon. It is possible that residues K3 and L21 mediate other activities of the VPg required for MNV infectivity, such as RNA encapsidation or modulation of translation initiation. The effects of the D48R mutant in the infectivity assay and the NS7$^{pol}$-VPg interaction assays are more difficult to explain, given that this mutant apparently retained wild-type infectivity but was unable to interact with the viral polymerase. We can only speculate that the interactions within the more-elaborate RNA replication complexes that form in infected cells might suppress the observed defect in the interaction of NS7$^{pol}$ and VPg detected by our assays.

By analogy with results for FMDV 3D$^{pol}$, which is structurally very similar to MNV NS7$^{pol}$ (Fig. 8A and B) (RMSD in backbone $C_\alpha$ positions, 3.9 Å) and binds FMDV VPg in an extended polypeptide conformation that positions the nucleotidylated Tyr (Tyr3) within the polymerase active site (75), we reasoned that the calicivirus VPg core would have to unfold to allow the nucleotide acceptor Tyr within helix α1 to adopt a similarly extended conformation. This hypothesis appeared to be consistent with observations that mutation of three Tyr residues in HuNV VPg (Y30A, Y41A, Y46A), all of which we would expect to destabilize the core of the protein, enhanced the nucleotidylation of the protein in *in vitro* assays (43). However, although alanine substitution of the equivalent residues in MNV VPg (F29, Y40, Y45) was confirmed to destabilize the protein core by NMR analysis (Fig. 6 and Table 2), these mutations generally impaired the interaction with the polymerase—although the effects for Y45A were relatively modest. The Y40F mutation, which resulted in a less-destabilized VPg core structure, showed evidence of good interaction with NS7$^{pol}$ and wild-type infectivity. Together, these findings appear to suggest that the stability of the VPg core structure contributes to VPg function.

However, a counterpoint to this interpretation is the observation that the Y45F mutation, which preserves the core structure, appeared to completely abrogate interaction with the polymerase and virus infectivity. It may be that Y45 has an important function beyond stabilization of the VPg core. Alternatively, the Y45F substitution may actually enhance the stability of the VPg core, which may impair its ability to interact functionally with the polymerase, assuming that interaction requires at least partial unfolding of the tertiary structure (see below). Finally, the mutation R32D that should disrupt formation of the salt bridge between the two core α-helices within MNV VPg did not impair infectivity (Table 2 and Fig. 7). Collectively, our results are consistent with the notion that the two-helix core structure of MNV VPg represents a finely balanced state of the VPg structure that may undergo modest conformational changes to participate in nucleotidylation by NS7$^{pol}$ and successful viral infection.

Manual docking trials with MNV VPg into the crystal structure of the MNV NS7$^{pol}$ (Fig. 8) suggest that, with minor side chain adjustments, there may be room in the substrate-binding channel to accommodate helix α1 in such a way that the Tyr26 acceptor is positioned in the active site, but only if this helix is detached from the VPg core. Alternatively, if the VPg core structure remains intact upon binding to the polymerase, the thumb and fingers domains of NS7$^{pol}$ would have to move apart to accommodate VPg in a productive complex. A proper test of these ideas awaits the determination of a structure of an NS7$^{pol}$-VPg complex. Until that time, the definition of the boundaries between structured and unstructured domains of the FCV and MNV VPg proteins and the fold of the structured cores reported here provide an improved

framework for the design of mutagenesis experiments to continue probing VPg function.

## ACKNOWLEDGMENTS

This work was funded by research grants from the Biotechnology and Biological Sciences Research Council (United Kingdom) to S.C. (reference number BB/J001708/1) and to I.G.G. and L.O.R. (reference numbers BB/I012303/1 and BB/I01232X/1), an Indiana Economic Development grant to C.K., and funding from the Wellcome Trust to I.G.G. I.G.G. is a Wellcome Senior Fellow (reference number WT097997MA). The work was also supported by the Intramural Research Program of the NIH, NIAID. E.N.L. was funded by a Wellcome Trust Ph.D. studentship (reference number 083248). J.R.B. and J.C.Y. were supported by Ph.D. studentships from the Medical Research Council, United Kingdom.

## REFERENCES

1. **Radford AD, Coyne KP, Dawson S, Porter CJ, Gaskell RM.** 2007. Feline calicivirus. Vet. Res. **38**:319–335.
2. **Patel MM, Widdowson MA, Glass RI, Akazawa K, Vinje J, Parashar UD.** 2008. Systematic literature review of role of noroviruses in sporadic gastroenteritis. Emerg. Infect. Dis. **14**:1224–1231.
3. **Scallan E, Hoekstra RM, Angulo FJ, Tauxe RV, Widdowson MA, Roy SL, Jones JL, Griffin PM.** 2011. Foodborne illness acquired in the United States—major pathogens. Emerg. Infect. Dis. **17**:7–15.
4. **Cheetham S, Souza M, Meulia T, Grimes S, Han MG, Saif LJ.** 2006. Pathogenesis of a genogroup II human norovirus in gnotobiotic pigs. J. Virol. **80**:10372–10381.
5. **Jung K, Wang Q, Kim Y, Scheuer K, Zhang Z, Shen Q, Chang K-O, Saif LJ.** 2012. The effects of simvastatin or interferon-α on infectivity of human norovirus using a gnotobiotic pig model for the study of antivirals. PLoS One **7**:e41619. doi:10.1371/journal.pone.0041619.
6. **Vashist S, Bailey D, Putics A, Goodfellow I.** 2009. Model systems for the study of human norovirus biology. Future Virol. **4**:353–367.
7. **Chaudhry Y, Skinner MA, Goodfellow IG.** 2007. Recovery of genetically defined murine norovirus in tissue culture by using a fowlpox virus expressing T7 RNA polymerase. J. Gen. Virol. **88**:2091–2100.
8. **Sosnovtsev S, Green KY.** 1995. RNA transcripts derived from a cloned full-length copy of the feline calicivirus genome do not require VpG for infectivity. Virology **210**:383–390.
9. **Ward VK, McCormick CJ, Clarke IN, Salim O, Wobus CE, Thackray LB, Virgin HW, IV, Lambden PR.** 2007. Recovery of infectious murine norovirus using pol II-driven expression of full-length cDNA. Proc. Natl. Acad. Sci. U. S. A. **104**:11050–11055.
10. **Wobus CE, Karst SM, Thackray LB, Chang KO, Sosnovtsev SV, Belliot G, Krug A, Mackenzie JM, Green KY, Virgin HW.** 2004. Replication of Norovirus in cell culture reveals a tropism for dendritic cells and macrophages. PLoS Biol. **2**:e432. doi:10.1371/journal.pbio.0020432.
11. **Yunus MA, Chung LM, Chaudhry Y, Bailey D, Goodfellow I.** 2010. Development of an optimized RNA-based murine norovirus reverse genetics system. J. Virol. Methods **169**:112–118.
12. **Kahan SM, Liu G, Reinhard MK, Hsu CC, Livingston RS, Karst SM.** 2011. Comparative murine norovirus studies reveal a lack of correlation between intestinal virus titers and enteric pathology. Virology **421**:202–210.
13. **Karst SM, Wobus CE, Lay M, Davidson J, Virgin HW, IV.** 2003. STAT1-dependent innate immunity to a Norwalk-like virus. Science **299**:1575–1578.
14. **McFadden N, Bailey D, Carrara G, Benson A, Chaudhry Y, Shortland A, Heeney J, Yarovinsky F, Simmonds P, Macdonald A, Goodfellow I.** 2011. Norovirus regulation of the innate immune response and apoptosis occurs via the product of the alternative open reading frame 4. PLoS Pathog. **7**:e1002413. doi:10.1371/journal.ppat.1002413.
15. **Belliot G, Sosnovtsev SV, Mitra T, Hammer C, Garfield M, Green KY.** 2003. In vitro proteolytic processing of the MD145 norovirus ORF1 nonstructural polyprotein yields stable precursors and products similar to those detected in calicivirus-infected cells. J. Virol. **77**:10957–10974.
16. **Blakeney SJ, Cahill A, Reilly PA.** 2003. Processing of Norwalk virus nonstructural proteins by a 3C-like cysteine proteinase. Virology **308**:216–224.
17. **Liu B, Clarke IN, Lambden PR.** 1996. Polyprotein processing in Southampton virus: identification of 3C-like protease cleavage sites by in vitro mutagenesis. J. Virol. **70**:2605–2610.
18. **Sosnovtsev SV, Belliot G, Chang KO, Prikhodko VG, Thackray LB, Wobus CE, Karst SM, Virgin HW, Green KY.** 2006. Cleavage map and proteolytic processing of the murine norovirus nonstructural polyprotein in infected cells. J. Virol. **80**:7816–7831.
19. **Ettayebi K, Hardy ME.** 2003. Norwalk virus nonstructural protein p48 forms a complex with the SNARE regulator VAP-A and prevents cell surface expression of vesicular stomatitis virus G protein. J. Virol. **77**:11790–11797.
20. **Nakamura K, Someya Y, Kumasaka T, Ueno G, Yamamoto M, Sato T, Takeda N, Miyamura T, Tanaka N.** 2005. A norovirus protease structure provides insights into active and substrate binding site integrity. J. Virol. **79**:13685–13693.
21. **Ng KK, Cherney MM, Vazquez AL, Machin A, Alonso JM, Parra F, James MN.** 2002. Crystal structures of active and inactive conformations of a caliciviral RNA-dependent RNA polymerase. J. Biol. Chem. **277**:1381–1387.
22. **Pfister T, Wimmer E.** 2001. Polypeptide p41 of a Norwalk-like virus is a nucleic acid-independent nucleoside triphosphatase. J. Virol. **75**:1611–1619.
23. **Sharp TM, Guix S, Katayama K, Crawford SE, Estes MK.** 2010. Inhibition of cellular protein secretion by Norwalk virus nonstructural protein p22 requires a mimic of an endoplasmic reticulum export signal. PLoS One **5**:e13130. doi:10.1371/journal.pone.0013130.
24. **Burroughs JN, Brown F.** 1978. Presence of a covalently linked protein on calicivirus RNA. J. Gen. Virol. **41**:443–446.
25. **Herbert TP, Brierley I, Brown TD.** 1997. Identification of a protein linked to the genomic and subgenomic mRNAs of feline calicivirus and its role in translation. J. Gen. Virol. **78**(Part 5):1033–1040.
26. **Schaffer FL, Ehresmann DW, Fretz MK, Soergel MI.** 1980. A protein, VPg, covalently linked to 36S calicivirus RNA. J. Gen. Virol. **47**:215–220.
27. **Daubert SD, Bruening G, Najarian RC.** 1978. Protein bound to the genome RNAs of cowpea mosaic virus. Eur. J. Biochem. **92**:45–51.
28. **Fuentes C, Bosch A, Pinto RM, Guix S.** 2012. Identification of human astrovirus genome-linked protein (VPg) essential for viral infectivity. J. Virol. **86**:10070–10078.
29. **Harding NE, Ito J, David GS.** 1978. Identification of the protein firmly bound to the ends of bacteriophage phi 29 DNA. Virology **84**:279–292.
30. **Lee YF, Nomoto A, Detjen BM, Wimmer E.** 1977. A protein covalently linked to poliovirus genome RNA. Proc. Natl. Acad. Sci. U. S. A. **74**:59–63.
31. **Mayo MA, Barker H, Harrison BD.** 1979. Evidence for a protein covalently linked to tobacco ringspot virus-RNA. J. Gen. Virol. **43**:735–740.
32. **Rekosh DM, Russell WC, Bellet AJ, Robinson AJ.** 1977. Identification of a protein linked to the ends of adenovirus DNA. Cell **11**:283–295.
33. **Salas M, Mellado RP, Vinuela E.** 1978. Characterization of a protein covalently linked to the 5′ termini of the DNA of Bacillus subtilis phage phi29. J. Mol. Biol. **119**:269–291.
34. **Siaw MF, Shahabuddin M, Ballard S, Shaw JG, Rhoads RE.** 1985. Identification of a protein covalently linked to the 5′ terminus of tobacco vein mottling virus RNA. Virology **142**:134–143.
35. **Chaudhry Y, Nayak A, Bordeleau ME, Tanaka J, Pelletier J, Belsham GJ, Roberts LO, Goodfellow IG.** 2006. Caliciviruses differ in their functional requirements for eIF4F components. J. Biol. Chem. **281**:25315–25325.
36. **Goodfellow I, Chaudhry Y, Gioldasi I, Gerondopoulos A, Natoni A, Labrie L, Laliberte JF, Roberts L.** 2005. Calicivirus translation initiation requires an interaction between VPg and eIF 4 E. EMBO Rep. **6**:968–972.
37. **Daughenbaugh KF, Fraser CS, Hershey JW, Hardy ME.** 2003. The genome-linked protein VPg of the Norwalk virus binds eIF3, suggesting its role in translation initiation complex recruitment. EMBO J. **22**:2852–2859.
38. **Leonard S, Chisholm J, Laliberte JF, Sanfacon H.** 2002. Interaction in vitro between the proteinase of Tomato ringspot virus (genus Nepovirus) and the eukaryotic translation initiation factor iso4E from Arabidopsis thaliana. J. Gen. Virol. **83**:2085–2089.
39. **Leonard S, Plante D, Wittmann S, Daigneault N, Fortin MG, Laliberte JF.** 2000. Complex formation between potyvirus VPg and translation eukaryotic initiation factor 4E correlates with virus infectivity. J. Virol. **74**:7730–7737.
40. **Leonard S, Viel C, Beauchemin C, Daigneault N, Fortin MG, Laliberte JF.** 2004. Interaction of VPg-Pro of turnip mosaic virus with the transla-

tion initiation factor 4E and the poly(A)-binding protein in planta. J. Gen. Virol. **85**:1055–1063.
41. **Wittmann S, Chatel H, Fortin MG, Laliberte JF.** 1997. Interaction of the viral protein genome linked of turnip mosaic potyvirus with the translational eukaryotic initiation factor (iso) 4E of Arabidopsis thaliana using the yeast two-hybrid system. Virology **234**:84–92.
42. **Velazquez-Moctezuma R, Banos-Lara MdR, Acevedo Y, Mendez E.** 2012. Alternative cell lines to improve the rescue of infectious human astrovirus from a cDNA clone. J. Virol. Methods **179**:295–302.
43. **Belliot G, Sosnovtsev SV, Chang KO, McPhie P, Green KY.** 2008. Nucleotidylylation of the VPg protein of a human norovirus by its proteinase-polymerase precursor protein. Virology **374**:33–49.
44. **Mitra T, Sosnovtsev SV, Green KY.** 2004. Mutagenesis of tyrosine 24 in the VPg protein is lethal for feline calicivirus. J. Virol. **78**:4931–4935.
45. **Subba-Reddy CV, Goodfellow I, Kao CC.** 2011. VPg-primed RNA synthesis of norovirus RNA-dependent RNA polymerases by using a novel cell-based assay. J. Virol. **85**:13027–13037.
46. **Rohayem J, Robel I, Jager K, Scheffler U, Rudolph W.** 2006. Protein-primed and de novo initiation of RNA synthesis by norovirus 3Dpol. J. Virol. **80**:7060–7069.
47. **Kaiser WJ, Chaudhry Y, Sosnovtsev SV, Goodfellow IG.** 2006. Analysis of protein-protein interactions in the feline calicivirus replication complex. J. Gen. Virol. **87**:363–368.
48. **Schein CH, Oezguen N, van der Heden van Noort GJ, Filippov DV, Paul A, Kumar E, Braun W.** 2010. NMR solution structure of poliovirus uridylyated peptide linked to the genome (VPgpU). Peptides **31**:1441–1448.
49. **Schein CH, Oezguen N, Volk DE, Garimella R, Paul A, Braun W.** 2006. NMR structure of the viral peptide linked to the genome (VPg) of poliovirus. Peptides **27**:1676–1684.
50. **Ferrer-Orta C, Arias A, Perez-Luque R, Escarmis C, Domingo E, Verdaguer N.** 2004. Structure of foot-and-mouth disease virus RNA-dependent RNA polymerase and its complex with a template-primer RNA. J. Biol. Chem. **279**:47212–47221.
51. **Hebrard E, Bessin Y, Michon T, Longhi S, Uversky VN, Delalande F, Van Dorsselaer A, Romero P, Walter J, Declerck N, Fargette D.** 2009. Intrinsic disorder in viral proteins genome-linked: experimental and predictive analyses. Virol. J. **6**:23.
52. **Grzela R, Szolajska E, Ebel C, Madern D, Favier A, Wojtal I, Zagorski W, Chroboczek J.** 2008. Virulence factor of potato virus Y, genome-attached terminal protein VPg, is a highly disordered protein. J. Biol. Chem. **283**:213–221.
53. **Rantalainen KI, Eskelin K, Tompa P, Makinen K.** 2011. Structural flexibility allows the functional diversity of potyvirus genome-linked protein VPg. J. Virol. **85**:2449–2457.
54. **Rantalainen KI, Uversky VN, Permi P, Kalkkinen N, Dunker AK, Makinen K.** 2008. Potato virus A genome-linked protein VPg is an intrinsically disordered molten globule-like protein with a hydrophobic core. Virology **377**:280–288.
55. **Jiang J, Laliberté J-F.** 2011. The genome-linked protein VPg of plant viruses—a protein with many partners. Curr. Opin. Virol. **1**:347–354.
56. **Zou P, Gautel M, Geerlof A, Wilmanns M, Koch MH, Svergun DI.** 2003. Solution scattering suggests cross-linking function of telethonin in the complex with titin. J. Biol. Chem. **278**:2636–2644.
57. **Bertani G.** 2004. Lysogeny at mid-twentieth century: P1, P2, and other experimental systems. J. Bacteriol. **186**:595–600.
58. **Marchant J, Sawmynaden K, Saouros S, Simpson P, Matthews S.** 2008. Complete resonance assignment of the first and second apple domains of MIC4 from Toxoplasma gondii, using a new NMRView-based assignment aid. Biomol. NMR Assign. **2**:119–121.
59. **Jung YS, Zweckstetter M.** 2004. Mars—robust automatic backbone assignment of proteins. J. Biomol. NMR **30**:11–23.
60. **Brunger AT, Adams PD, Clore GM, DeLano WL, Gros P, Grosse-Kunstleve RW, Jiang JS, Kuszewski J, Nilges M, Pannu NS, Read RJ, Rice LM, Simonson T, Warren GL.** 1998. Crystallography & NMR system: a new software suite for macromolecular structure determination. Acta Crystallogr. D. **54**:905–921.
61. **Linge JP, Williams MA, Spronk CAEM, Bonvin AMJJ, Nilges M.** 2003. Refinement of protein structures in explicit solvent. Proteins **50**:496–506.
62. **Rieping W, Habeck M, Bardiaux B, Bernard A, Malliavin TE, Nilges M.** 2007. ARIA2: automated NOE assignment and data integration in NMR structure calculation. Bioinformatics **23**:381–382.
63. **Shen Y, Delaglio F, Cornilescu G, Bax A.** 2009. TALOS plus: a hybrid method for predicting protein backbone torsion angles from NMR chemical shifts. J. Biomol. NMR **44**:213–223.
64. **Bhattacharya A, Tejero R, Montelione GT.** 2007. Evaluating protein structures determined by structural genomics consortia. Proteins **66**:778–795.
65. **Sosnovtsev SV, Garfield M, Green KY.** 2002. Processing map and essential cleavage sites of the nonstructural polyprotein encoded by ORF1 of the feline calicivirus genome. J. Virol. **76**:7060–7072.
66. **Ohnishi M, Urry DW.** 1969. Temperature dependence of amide proton chemical shifts: the secondary structures of gramicidin S and valinomycin. Biochem. Biophys. Res. Commun. **36**:194–202.
67. **Lee JH, Alam I, Han KR, Cho S, Shin S, Kang S, Yang JM, Kim KH.** 2011. Crystal structures of murine norovirus-1 RNA-dependent RNA polymerase. J. Gen. Virol. **92**:1607–1616.
68. **Ng KK, Pendas-Franco N, Rojo J, Boga JA, Machin A, Alonso JM, Parra F.** 2004. Crystal structure of Norwalk virus polymerase reveals the carboxyl terminus in the active site cleft. J. Biol. Chem. **279**:16638–16645.
69. **Zamyatkin DF, Parra F, Alonso JM, Harki DA, Peterson BR, Grochulski P, Ng KK.** 2008. Structural insights into mechanisms of catalysis and inhibition in Norwalk virus polymerase. J. Biol. Chem. **283**:7705–7712.
70. **Han KR, Choi Y, Min BS, Jeong H, Cheon D, Kim J, Jee Y, Shin S, Yang JM.** 2010. Murine norovirus-1 3Dpol exhibits RNA-dependent RNA polymerase activity and nucleotidylylates on Tyr of the VPg. J. Gen. Virol. **91**:1713–1722.
71. **Subba-Reddy CV, Yunus MA, Goodfellow IG, Kao CC.** 2012. Norovirus RNA synthesis is modulated by an interaction between the viral RNA-dependent RNA polymerase and the major capsid protein, VP1. J. Virol. **86**:10138–10149.
72. **Goodfellow I.** 2011. The genome-linked protein VPg of vertebrate viruses—a multifaceted protein. Curr. Opin. Virol. **1**:355–362.
73. **Eskelin K, Hafrén A, Rantalainen KI, Mäkinen K.** 2011. Potyviral VPg enhances viral RNA translation and inhibits reporter mRNA translation *in planta*. J. Virol. **85**:9210–9221.
74. **Dunham DM, Jiang X, Berke T, Smith AW, Matson DO.** 1998. Genomic mapping of a calicivirus VPg. Arch. Virol. **143**:2421–2430.
75. **Ferrer-Orta C, Arias A, Agudo R, Pérez-Luque R, Escarmís C, Domingo E, Verdaguer N.** 2006. The structure of a protein primer-polymerase complex in the initiation of genome replication. EMBO J. **25**:880–888.